Surface Discharge Detection and Severity Assessment of Printed Circuit Boards for Electric Aircraft Using Fluorescent Fiber

Zang, Yiming; Niasar, Mohamad Ghaffarian; Li, Ze; Li, Yaocheng; Qian, Qinglin; Jiang, Xiuchen; Vaessen, Peter

DOI
10.1109/TDEI.2024.3353171

Publication date
2024

Document Version
Final published version

Published in
IEEE Transactions on Dielectrics and Electrical Insulation

Citation (APA)
Zang, Y., Niasar, M. G., Li, Z., Li, Y., Qian, Q., Jiang, X., & Vaessen, P. (2024). Surface Discharge Detection and Severity Assessment of Printed Circuit Boards for Electric Aircraft Using Fluorescent Fiber. *IEEE Transactions on Dielectrics and Electrical Insulation*, *31*(6), 3057-3066. https://doi.org/10.1109/TDEI.2024.3353171

Surface Discharge Detection and Severity Assessment of Printed Circuit Boards for Electric Aircraft Using Fluorescent Fiber

Yiming Zang, Mohamad Ghaffarian Niasar, Ze Li, Yaocheng Li, Qinglin Qian, Xiuchen Jiang, and Peter Vaessen, *Member, IEEE*

***Abstract*— More and more printed circuit boards (PCBs) will be used in electric aircraft to achieve higher power density of the on-board electric system, while PCBs in aircraft are more likely to generate partial discharges (PDs) due to external factors such as compact structure and low air pressure. Therefore, this article proposes a fluorescent fiber-based method for detecting and evaluating PDs on PCBs. The detection method is effectively immune against the presence of the electromagnetic, acoustic, and vibration interference. Based on the optical detection, the evolution regularities of PCB surface appearance changes, optical PRPD patterns, and optical pulses during the aging process of PCB under different air pressure are analyzed in this article. Then, 12 assessment features are extracted for the PD aging process, and the contribution of these 12 features to the severity assessment at different air pressures is obtained using the minimal-redundancy-maximal-relevance (mRMR) algorithm. Finally, different numbers of PD features are tested for PD severity assessment by the support vector machine (SVM) algorithm. The evaluation results show that the severity assessment method proposed in this article can achieve an assessment accuracy of at least 91.1% and up to 94.4% under all three air pressures, which has good application and guidance value.**

***Index Terms*— Electric aircraft, fluorescent fiber, partial discharge (PD), printed circuit boards (PCB), severity assessment.**

I. Introduction

With the increased demand for eco-friendly and high energy efficiency in aircraft, more-/all-electric aircraft (MEA/AEA) are increasingly being investigated to replace the reliance on traditional hydraulic, mechanical, and pneumatic aviation systems [1], [2]. Printed circuit boards (PCBs) are widely used in MEA/AEA as a key component to energize the electronic system [3]. However, a higher voltage level, higher voltage frequency (more than 50 Hz), and more compact circuit designs are required in MEA/AEA to achieve a high-power density, which means PCBs need to be subjected to more severe electrical stress [4], [5], [6]. Since aircraft operate at high altitude, the low air pressure operating environment can result in formation of partial discharges (PDs) at lower electric stress which exacerbate the deterioration of insulation on PCBs, and can lead to increased risk of failure [7].

PD is one of the important signs of a decrease in insulation performance for PCBs before a complete breakdown, known as a "silent killer" of electronic systems. The PD detection and severity assessment of PCBs in MEA/AEA can effectively reflect the insulation status and risk level [8]. The current PD detection methods for MEA/AEA mainly include the ultrahigh-frequency (UHF) method, acoustic method, and high-frequency current method [9], [10], [11]. However, the harsh environment in MEA/AEA such as electromagnetic, acoustic, and vibration interferences during the operation of aircraft can seriously affect the detection performance of existing methods. Therefore, this article proposes a PD detection method based on the fluorescent fiber and avalanche photodetector (APD), which can effectively avoid interference sources in MEA/AEA. Furthermore, the flexible fluorescent fiber can be distributed in almost all positions of the PCBs, thus enabling more complete and reliable PD detection.

In addition, there are very few studies on PD for PCBs with conformal coating in the low air pressure environment of aircraft, in which there is essentially no research based on optical PD signals. Emersic et al. [12], [13] studied the PD inception voltage and surface electric field of PCBs under low air pressure at different temperatures and presented microscopic pictures of PCBs under continuous aging voltage. Karady et al. [14] investigated the changes in appearance of the deterioration process of corona discharge on PCBs at low air pressure. Zeynali et al. [15] studied the PD phenomenon of coated PCBs in aircraft under different contamination conditions, but did not involve the aging process of PD at low air pressure. The existing work lacked the investigation of the evolution of electrical characteristics during PD, thus failing

Manuscript received 8 October 2023; revised 18 December 2023; accepted 6 January 2024. Date of publication 11 January 2024; date of current version 19 December 2024. This work was supported in part by the Startup Fund for Young Faculty at Shanghai Jiao Tong University (SJTU) under Grant 23X010502189. *(Corresponding author: Yiming Zang.)*

Yiming Zang, Ze Li, Yaocheng Li, Qinglin Qian, and Xiuchen Jiang are with the Department of Electrical Engineering, Shanghai Jiao Tong University, Shanghai 200240, China (e-mail: zangyiming@sjtu.edu.cn; lize123@sjtu.edu.cn; yaocheng.li@sjtu.edu.cn; qianqinglin@sjtu.edu.cn; xcjiang@sjtu.edu.cn).

Mohamad Ghaffarian Niasar and Peter Vaessen are with the Electrical Sustainable Energy Department, Delft University of Technology, 2628 Delft, The Netherlands (e-mail: M.GhaffarianNiasar@tudelft.nl; P.T.M.Vaessen@tudelft.nl).

Color versions of one or more figures in this article are available at https://doi.org/10.1109/TDEI.2024.3353171.

Digital Object Identifier 10.1109/TDEI.2024.3353171

to provide a timely and effective assessment to the insulation degradation state of the PCBs.

Our research group has also carried out previous research related to the optical detection of PD on PCB, but only on the detection method and signal characteristics [16]. In this article, we carry out further research about PD severity assessment based on our previous optical detection platform. Therefore, the PD aging behavior on PCBs under different air pressure, including PCB surface appearance changes, PD pulse interval, phase-resolved PD (PRPD) pattern, and PD pulse amplitude, are investigated in this article based on the optical PD detection method. Twelve PD features at different aging stages are extracted to comprehensively characterize the insulation degradation process of PCBs. Moreover, this article proposes to use the minimal-redundancy-maximal-relevance (mRMR) algorithm to rank the contribution of 12 PD features for the assessment, which more objectively obtains the influence of the feature number on the severity assessment accuracy. Finally, the support vector machine (SVM) algorithm is used to train the PD feature set and recognize the aging stage, so as to achieve an accurate and high-efficient assessment of the PD severity for PCBs. The fluorescent fiber-based detection method proposed in this article not only obtains the characteristic evolution of the optical PD behavior of PCBs in aircraft, but also provides new solution ideas for PCBs insulation state assessment and qualification control before PCBs are put into service.

II. PD Detection Based on the Fluorescent Fiber and APD

A. Detection Theory of Fluorescent Fiber

Fluorescent fiber is a light-sensitive material that is well insulated, flexible, and immune to electromagnetic and acoustic interferences, which is well compatible with the working environment of PCBs in aircraft. Traditional quartz optical fiber with outer cladding requires a certain angle of incidence to receive light signals for transmission. Differently, fluorescent fiber can receive light from any incident angle, which effectively improves the range and sensitivity of detection [17]. In particular, PCBs may have components that obscure the optical PD signal, while the flexible arrangement of fluorescent fibers can reach everywhere on the PCB, achieving more thorough detection.

The fluorescent fiber is filled with a fluorescent substance that absorbs incident light of a specific spectrum. When the incident light meets the absorption spectrum of the fluorescent material, the fluorescent material absorbs the incident photons to reach the excited state. The fluorescent substance in the excited state will return to the steady state due to instability, and this process will emit light of longer wavelengths to propagate in the fiber core. The light satisfying the total reflection conditions of the fiber core-packet layer interface propagates forward along the axial direction of the fiber and is finally detected at the terminal face of the fiber, as shown in Fig. 1.

Since there is a Stoke Shift phenomenon in the emission of photons from fluorescent substances, the emission spectrum of fluorescent substances is about 100–200 nm longer than the excitation spectrum. This requires the excitation spectrum of the fluorescent fiber to meet the emission spectrum of the light source to be sensed (PD emission spectrum), and the emission spectrum of the fluorescent fiber needs to meet the detection response spectrum of the APD.

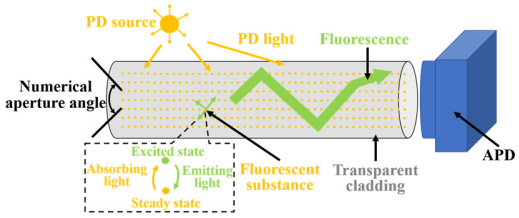

Fig. 1. Schematic of the fluorescent fiber sensing principle.

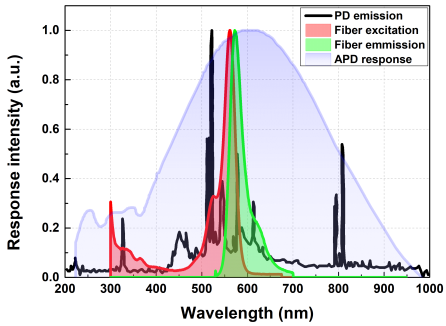

Fig. 2. Response intensity distribution of different spectra.

B. Optical Sensing Parameter Selection

Based on the detection principle of fluorescent fiber, APD is selected as the sensor for photoelectric conversion in this article. Compared with other photoelectric conversion sensors mainly used in the laboratory (e.g., photomultiplier tube, spectrometer, etc.), APD has the advantages of small size, easy installation and no high-power supply, which can be more convenient for PD detection in reality. In order to ensure the effectiveness of the entire optical detection, it is necessary to match the PD emission spectrum, fluorescence fiber excitation spectrum, fluorescence fiber emission spectrum, and APD response spectrum with each other. Since most of the PDs on PCBs are occurred between copper tracks, the PD spectrum for PCBs is mostly distributed between 300 and 650 nm according to the related work [18]. Accordingly, we selected the Alexa Fluor 546 fluorescent fiber and APD130A2 whose main wavelength bands can match the other spectrums, and their main spectral distributions are shown in Fig. 2. Due to the different standards for measuring different spectral intensities, the spectral response intensities are normalized in Fig. 2. Fig. 2 shows that the distribution of the four spectrums almost satisfies the above-mentioned principle of mutual matching, which can ensure a high detection efficiency.

III. Experimental Design and Performance Testing

A. PCB Sample Design

In this work, three typical track structures commonly found on PCBs are designed to perform PD experiments with the dimensions shown in Fig. 3.

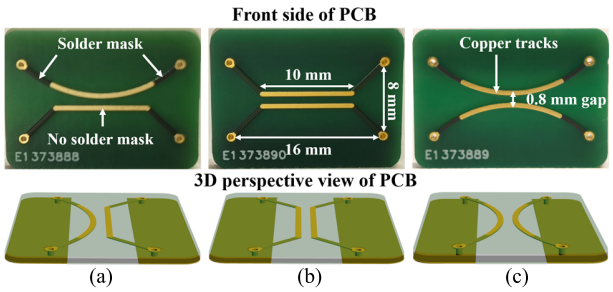

Fig. 3. Schematic of the three PCB structures. (a) CL. (b) LL. (c) CC.

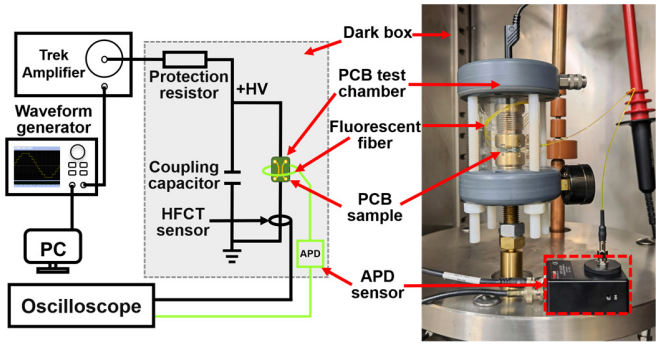

Fig. 4. PCB optical PD detection experiment platform.

These three structures are fundamentally representative of the various conductor conditions on the PCBs where PD may occur. These three PCB structures are called Curve-Line (CL), Line-Line (LL), and Curve-Curve (CC) in this article. The shortest gap between two tracks in each structure is 0.8 mm at the center of the track, which meets the industry test standard for PCBs (IPC 2221-A). The track material in the middle area is copper without solder mask coverage. The PCB substrate material is FR4. Four through holes are used to connect the copper tracks on back of the PCB for applying voltage. All other areas of the PCBs are covered with solder mask.

Since PCBs are subjected to electrical, mechanical, thermal, and radiation stresses in aircraft, most of them are now covered with "conformal coating" to protect PCBs for stable operation in harsh environments. According to the standard IPC-CC-830, the conformal coating is a homogeneous, transparent polymer, and free of harmful substances. Silicone is a kind of conformal coating, which is widely used for PCBs in aircraft because of its excellent thermal, humidity, and chemical resistance along with good dielectric properties.

In the process of making the PCB experimental samples, PCB samples are rinsed with deionized water for 5 min at 20 °C ± 1 before being coated with conformal coating. Next, PCB samples are dipped in isopropyl alcohol for a further 4 min and are dried in a dust-free fume hood. Then, the PCB surface was covered with conformal coating by spraying in a dust-free fume hood. Finally, the PCB was dried in an airtight drying oven at 90 °C for 2 h to obtain the final experimental PCB. Silicone FSC 400 is used in this article by spraying on the surface of PCBs. Due to some randomness in the thickness of the sprayed conformal coating, a batch of at least 20 PCB samples are uniformly made. PCB samples with the thickness of the conformal coating between 30 and 50 μm are selected for the experiment by micrometer [19].

B. Experiment Setup

In order to simulate the low air pressure working environment in aircraft, the PD experimental platform of PCBs shown in Fig. 4 is built in this article. A vacuum pump is used to vary the air pressure in the test chamber at 1 atmosphere (atm), 0.5 and 0.1 atm, respectively. The fluorescent fiber with yellow appearance is wrapped around the inside of the test chamber. A waveform generator and Trek 30/20A HV amplifier are used to generate the high voltage. Since the increase of voltage frequency can accelerate the degradation of insulation, and considering the typical voltage types applied in MEA/AEA, ac 400 Hz is selected to apply to the copper tracks in this article [20]. Although 400 Hz is used, in the future, inside dc/dc converter much higher frequencies will be used at 10 s of kHz. In this article, we take 400 Hz, which is currently used more often, as an example, and related methods can also be applied in the future. A high frequency current transformer (HFCT) is also used for the PD detection to perform a comparative test. The entire experimental equipment is placed in a dark box that is impervious to light. The oscilloscope is Picoscope 6.0.

In this article, the PCBs of all three structures are subjected to PD experiments at three different air pressures. The PD aging voltage of the PCB is not suitable to be too high or too low. When the PD aging voltage is too low, the signal is not stable, and the aging breakdown time required is too long, which is not conducive to experimental observation. When the PD aging voltage is too high, the breakdown time of the PCB is too short, which is not conducive to the collection and accumulation of PD data during the aging process. In addition, the inception voltage of PD (PDIV) of PCBs may be different under different air pressure, different thickness of conformal coating, and different structures. Therefore, after many experimental attempts of PCB breakdown, the aging voltage is set to 1.1 times of PDIV for all PCB samples during the PD aging experiment, ensuring the uniformity of the experiment. The PD pulses are recorded from the start of the 1.1 PDIV until the breakdown of the PCB sample. For all the experimental procedures, a small data sample containing 1000 PD pulses is recorded for each PCB sample every 15 s on average, and a large data sample containing 10 000 PD pulses is recorded every 200 s on average for each PCB sample. The time required to collect each data set is also recorded.

C. Performance Testing of Optical Detection

In order to verify the performance of the proposed method based on fluorescent fiber and APD, HFCT signals are collected simultaneously during the PD experiments as a control. In the preexperiment, 100 000 PD pulses are collected during the aging process. The minimum detection sensitivity of the HFCT detection system in this article can reach about 2 pC. In this article, each HFCT pulse can be collected corresponding to an optical pulse, showing that there is no missing detection phenomenon. This indicates that the

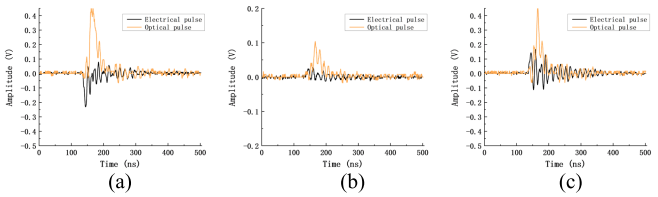

Fig. 5. Simultaneous acquisition of optical and electrical pulses of PCB PD at three air pressures. (a) 1 atm. (b) 0.5 atm. (c) 0.1 atm.

TABLE I
PD SEVERITY DIVISION STANDARD

Severity stage	Risk level	Stage division
S1	Attention risk (Att)	PD starting time ~ 1/3 T_b
S2	Moderate risk (Mod)	1/3 T_b ~ 2/3 T_b
S3	Dangerous risk (Dan)	2/3 T_b ~ Breakdown time

method proposed in this article can effectively detect the PD occurrence. Fig. 5 illustrates the synchronized acquisition waveforms of the PD optical pulses and electrical pulses (collected by HFCT) for the three air pressure conditions, further demonstrating the effectiveness of the optical detection method at different air pressures. Unlike the electrical signals which have positive polarity and negative polarity, the optical PD pulse has only positive polarity.

D. Division of the PD Severity for PCBs

Currently, there is no division standard for the PD severity on PCBs. A reasonable method to classify the severity of PD on PCBs can facilitate the evaluation of insulation deterioration state and quality verification testing of PCBs, which is necessary in practice. Therefore, this article proposes a severity division method based on aging time, as shown in Table I. T_b denotes the time required for a PCB sample to fully breakdown from the starting time of PD aging. The entire aging time T_b is equally divided into three stages. The severity division method is based on the time required for breakdown, and can accordingly represent the risk of complete failure of the PCB insulation. Severity assessments are based on the division standards.

IV. PD Characterization at Different Air Pressures and Severity

Through PD experiments on PCBs of different structures, it is found that the PCBs of these three typical structures in this article respond essentially the same to changes in different experimental conditions. There are only some differences in the magnitude of changes between different structures, but the basic law is generally the same. Therefore, in this section, the PCB structure of "LL" type is used as an example to analyze the PD characteristics at different air pressures and different severity stages.

A. Observation of PD Aging Process

The appearance changes on the copper track of PCB during PD aging, captured by a microscope, are shown in Fig. 6.

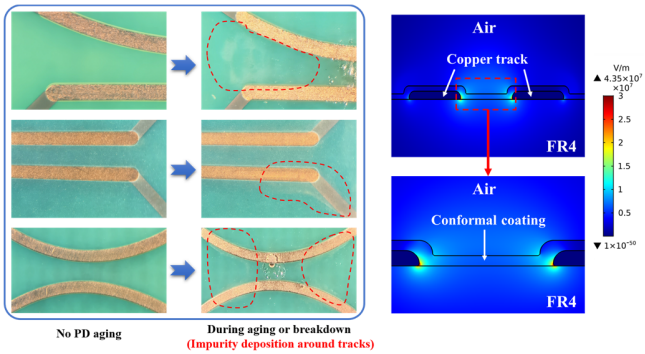

Fig. 6. Micrographic changes of PCB surface during PD aging process (left) and electric field simulation (right).

As can be seen from the micrographs, the PCB surface covered with conformal coating is very clean before the PD aging. When the PCB is aged under PD for a period of time or after aging breakdown, it is found that tiny white impurities appear in the surrounding area of the PCB copper tracks. These impurity deposits appear on the surface of the conformal coating and can be wiped away. Relatively more impurities are deposited between the two tracks, forming an impurity channel. At the same time, we simulate the electric field distribution in the center cross section of the PCB during the aging process according to the actual size of the PCB in COMSOL software, as shown in Fig. 6. Through the simulation, it is found that the electric field is maximum at two intersections of three media, which are the intersection of FR4, conformal coating, and copper tracks and the intersection of air, conformal coating, and copper row. However, since the insulation strength of the air is much lower than that of the conformal coating, the PD is a surface discharge occurring on the surface of the PCB. Comparing the distribution of the electric field with the impurity deposition observed under the microscope, it can be shown that the impurity deposition is the attachment of free aerosol particles in the air around the tracks under the action of electric field. Since the exact chemical composition of the impurity could not be clarified during this research, its effect on PD aging remains to be further explored.

In Fig. 6, when the PCB aging to breakdown, it can be seen that the copper tracks and the conformal coating are significantly damaged. The conformal coating around the location where the breakdown occurred is corroded and melted. The breakdown can also affect the safety of devices around the breakdown point when it is severe. Therefore, it is important to assess the insulation state of the PCB surface by PD.

B. PRPD Patterns Under Different Conditions

In order to study the process of PD aging of PCBs at different air pressures, PRPD patterns are used in this article to describe the changes in phase distribution for different PD severities, as shown in Fig. 7. PRPD patterns are φ-n plots, where the horizontal coordinate φ is the phase of ac applied voltage and the vertical coordinate n is the number of PDs at that phase. One "LL" type PCB sample is selected for aging experiments at each air pressure. For each air pressure

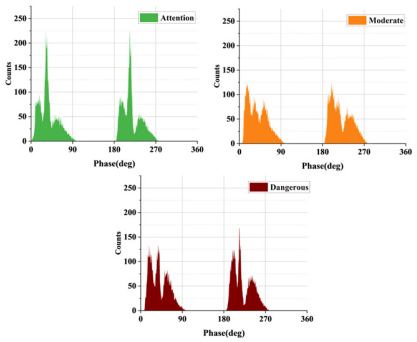

Severity	Main phase distribution	Total PD pulses number
Attention	0° ~ 111°	5076
	182° ~ 286°	4924
Moderate	3° ~ 114°	5015
	183° ~ 290°	4985
Dangerous	5° ~ 111°	5032
	185° ~ 285°	4968

(a)

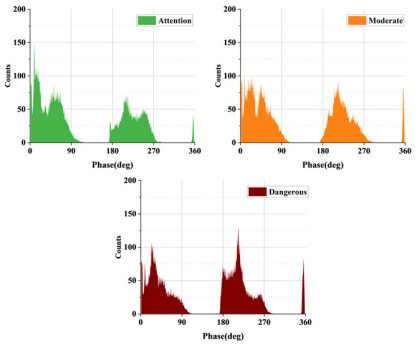

Severity	Main phase distribution	Total PD pulses number
Attention	0° ~ 128°	6011
	166° ~303°	3842
	351° ~ 360°	147
Moderate	0° ~ 118°	5529
	171° ~ 307°	4131
	351° ~ 360°	332
Dangerous	0° ~ 123°	4560
	170° ~ 300°	5014
	350° ~ 360°	412

(b)

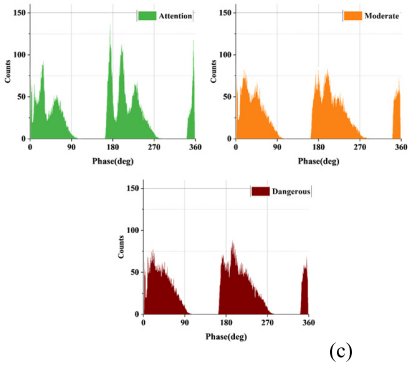

Severity	Main phase distribution	Total PD pulses number
Attention	0° ~ 116°	3741
	163° ~300°	5362
	341° ~ 360°	886
Moderate	0° ~ 111°	4044
	162° ~ 294°	4884
	340° ~ 360°	936
Dangerous	0° ~ 114°	4054
	163° ~ 293°	5054
	341° ~ 360°	819

(c)

Fig. 7. PRPD patterns of PCBs with different PD severity at three air pressures. (a) 1 atm. (b) 0.5 atm. (c) 0.1 atm.

in Fig. 7, each PRPD pattern represents the average phase distribution per 10 000 PD pulses at that severity stage.

In Fig. 7, the phase distribution of PD on PCBs is mostly in the positive and negative half-cycle of the voltage rise phase. The PRPD patterns with different severity stages at the same air pressure have significant differences in the phase distribution. As a whole, the distribution of the number of PD pulses varies significantly with severity, while the overall distribution range of the phase is basically unchanged at the same air pressure. According to the previous analysis, one of the reasons for the variation of the PRPD patterns at different severity stages may be the local distortion of the electric field caused by the deposition of impurities on the PCB surface. Also, the impurities deposition changes the conductivity of the PCB surface, which has an impact on both the migration and accumulation of charges on the surface. In addition, a slight local temperature rise and decomposition of the insulation material can also occur due to long PD aging. The combined effect of these multiple factors leads to a certain regular

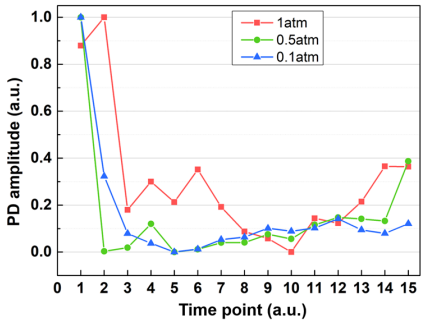

Fig. 8. Relationship between optical PD amplitude and aging time.

change in the PRPD patterns of PCBs with the change in PD severity, which provides a reference for extracting the PD characteristics at different stages for severity assessment.

In addition, for the PRPD patterns at the same PD severity in different air pressures, it can be seen from Fig. 7 that the phase distribution of PD gradually widens in both positive and negative half-cycles as the air pressure decreases (from 1 to 0.1 atm). In particular, the PD phase distribution widens more obviously in the phase region where the voltage polarity exchanges between positive and negative. This is due to fact that the PD on PCBs also follow the laws of Paschen's Curves. When the air pressure decreases, the minimum field threshold of PD on the surface of the PCB will be reduced, according to the right side of the Paschen's curve minimum. Therefore, the voltage distribution to meet the PD occurrence conditions becomes wider, corresponding to a wider phase distribution. Especially in the area of voltage polarity change, the surface charge accumulated under the previous voltage polarity will enhance the electric field under the next opposite polarity voltage, thus more likely to generate PD at this phase range.

C. PD Pulse Characteristics

Fig. 8 records the optical PD pulse amplitude versus PD aging time for the three air pressures. The trend of the PD intensity can be determined by observing the change in the optical PD pulse amplitude. The coating thickness is difficult to control precisely, and the difference of a few micrometers in thickness can make the PD inception voltage, aging time, and PD intensity change [9]. In this article, PD aging experiments are conducted on at least three PCB samples at each air pressure. It is found that although there are differences in aging time and PD amplitude for different samples at the same air pressure, the trend of the optical PD amplitude obtained at the same air pressure is basically similar. Therefore, considering the differences in aging time scales and PD amplitude ranges under different air pressures, a representative group of samples are selected to normalize their optical PD amplitudes and aging times to obtain Fig. 8. The time unit in Fig. 8 represent 15 typical time points selected uniformly from the beginning time of aging to the end time of breakdown process for each air pressure condition, which enables a more intuitive comparison of the overall trend.

In Fig. 8, the optical PD pulse amplitude decreases significantly first for all three air pressures as the aging time

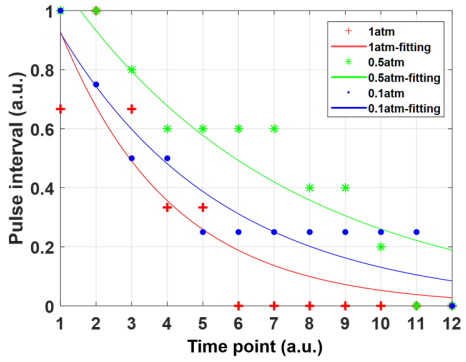

Fig. 9. Relationship between PD pulse interval and aging time.

increases. During the subsequent aging process, the optical PD pulse amplitude at 0.5 and 0.1 atm air pressure tends to increase slowly until breakdown. However, the optical PD pulse amplitude at 1 atm showed a fluctuating decreasing trend during the subsequent aging process until a significant increase before breakdown. This is probably due to the low number of discharges at the beginning of aging and the low surface charge accumulated near the PCB copper tracks. With the increasing number of discharges, a large amount of surface charge will appear on the PCB surface to weaken the PD electric field, which leads to a decrease in discharge intensity. However, as the PD aging continues to intensify, the degradation of the PCB insulation strength and the deposition of surface impurities will make the PD field becomes larger, so that the discharge amplitude tends to rise before the near breakdown.

The fit relationship between the aging time and the time interval between two consecutive PD pulses represented in Fig. 9. Since the aging durations of different samples differ, the pulse intervals also differ in order of magnitude at different time stages, which is difficult to demonstrate in one coordinate system. Therefore, considering the comparison between different air pressures, the time and pulse interval of each sample are normalized in this article, and an exponential fit is performed to better represent the variation trend, as shown in Fig. 9. The time unit in Fig. 9 represent 12 typical time points selected uniformly from the beginning time of aging to the end time of breakdown process for each air pressure condition. It can be seen from Fig. 9 that the time interval of PD pulses at all three air pressures gradually becomes shorter as the aging time increases, in which the time interval at 1 atm has the fastest decreasing trend. This phenomenon indicates that as PD aging proceeds, the frequency of PD pulses gradually increases, which might be related to the PCB surface modification due to the energy released by the PD aging.

Therefore, the analysis shows that the amplitude and time interval of PD pulses are closely related to PD aging, which provides support to further study the PD aging mechanism.

V. PD Severity Assessment

A. Severity Assessment Features

According to the analysis of the change of regularity of various types of PD characteristics during the aging process of PCB, this article proposes 12 evaluation features that can comprehensively reflect the PD severity at the statistical aspect. In the process of feature extraction, every data sample consisting of 1000 PD pulses are converted into φ-n pattern and φ-q pattern, which are the distribution of the number of PD pulses (n) and optical PD pulse amplitude (q) on the ac phase (φ). Both φ-n pattern and φ-q pattern are one kind of PRPD pattern. Then 12 feature parameters are extracted from each data sample (including 1000 PD pulses) to form the evaluation feature vector. The 12 features parameters are as follows:

1) *Skewness:* $\mathrm{Sk}^{+}_{\varphi-n}, \mathrm{Sk}^{-}_{\varphi-n}, \mathrm{Sk}^{+}_{\varphi-q}, \mathrm{Sk}^{-}_{\varphi-q}$
$\mathrm{Sk}^{+}_{\varphi-n}, \mathrm{Sk}^{-}_{\varphi-n}, \mathrm{Sk}^{+}_{\varphi-q}, \mathrm{Sk}^{-}_{\varphi-q}$ represent the skewness within the positive and negative half cycle of the φ-n pattern and φ-q pattern, respectively.
2) *Kurtosis:* $\mathrm{Ku}^{+}_{\varphi-n}, \mathrm{Ku}^{-}_{\varphi-n}, \mathrm{Ku}^{+}_{\varphi-q}, \mathrm{Ku}^{-}_{\varphi-q}$
$\mathrm{Ku}^{+}_{\varphi-n}, \mathrm{Ku}^{-}_{\varphi-n}, \mathrm{Ku}^{+}_{\varphi-q}, \mathrm{Ku}^{-}_{\varphi-q}$ represent the kurtosis within the positive and negative half cycle of the φ-n pattern and φ-q pattern, respectively.
3) *Average Correlation Coefficient:* $\mathrm{CC}_{\varphi-n}, \mathrm{CC}_{\varphi-q}$
$\mathrm{CC}_{\varphi-n}, \mathrm{CC}_{\varphi-q}$ are the average correlation coefficient of the φ-n and φ-q patterns, respectively.
4) *PD Number Difference:* $\mathrm{Nu}_{\varphi-n}$
$\mathrm{Nu}_{\varphi-n}$ is the difference between the total number of PD pulses in the positive half-cycle (Nu^{+}) and negative half-cycle (Nu^{-}) of the φ-n pattern.
5) *PD Amplitude Difference:* $\mathrm{Am}_{\varphi-q}$
$\mathrm{Am}_{\varphi-q}$ indicates the difference in the sum of the positive half-cycle (Am^{+}) and negative half-cycle (Am^{-}) PD amplitudes in the φ-q pattern.

These 12 statistical parameters are used as features for the PD severity assessment of PCBs.

B. Feature Contribution Ranking by mRMR

The 12 features extracted above characterize the evolution of PD severity from different perspectives, but some of them may have overlapping information or low relevance to the severity stages. Therefore, in order to evaluate the validity of each feature, this article proposes to mine and evaluate all features using the mRMR algorithm to obtain the contribution ranking of these features.

Mutual information in the RMR algorithm is defined as the correlation and redundancy relationship between two feature variables [21], defined as

$$I(x, y) = \iint p(x, y) \frac{p(x, y)}{p(x)p(y)} dxdy \tag{1}$$

where x and y are two feature variables, $p(x)$, $p(y)$, and $p(x, y)$ are their probability density and joint probability density.

The principle of maximum relevance refers to the feature variables having maximum dependence on the corresponding categorical labels, expressed as

$$\max D(S, c), \quad D = \frac{1}{|S|} \sum_{f_i \epsilon S} I(f_i, c) \tag{2}$$

where S is the feature set, $|S|$ is the size of S, f_i is the ith feature, and c is the categorical label.

The minimum redundancy criterion is the minimum intercorrelation between all feature variables, expressed as

$$\min R(S),\ R = \frac{1}{|S|^2}\sum_{f_i,f_j\in S} I(f_i, f_j) \tag{3}$$

where f_i and f_j are the i and jth features.

The mRMR algorithm is a combination of the maximum relevance criterion and the minimum redundancy criterion described above. The combination of D and R is achieved by defining an operator $\Phi(D, R)$, which allows the results of D and R to reach a simultaneous optimum

$$\max \Phi(D, R), \quad \Phi = D - R. \tag{4}$$

In finding the optimal solution, the optimal features can be found by incremental search based on $\Phi(D, R)$. Suppose there is a feature set S_{m-1} containing m-1 features. The mth feature satisfying the optimal condition can be found by the following criterion:

$$\max_{f_j\epsilon X - S_{m-1}}\left[I(f_i, c) - \frac{1}{m-1}\sum_{x_i\epsilon S_{m-1}} I(f_i, f_j)\right] \tag{5}$$

where f_j is a feature variable that belongs to the original feature set X but does not belong to S_{m-1}.

The calculation of the mRMR algorithm enables the ranking of the features in the feature set in terms of their contribution, thus obtaining which features are relatively more beneficial for PD severity assessment.

C. PD Severity Assessment by SVM

In this article, the SVM algorithm is proposed to perform pattern recognition on the collected PD dataset. The features in the dataset are the feature sets selected after ranking according to the mRMR algorithm. The classification labels in the dataset are three severity stages (Att, Mod and Dan). In order to eliminate the effect of different physical units between different feature variables, the selected feature set is normalized as follows before performing the pattern recognition:

$$f_i^* = \frac{f_i - f_{\min}}{f_{\max} - f_{\min}} \tag{6}$$

where f_i^* and f_i are the normalized feature and the original feature respectively and $f_{\max}$ and $f_{\min}$ are the maximum and minimum values of the original feature.

The SVM finds a hyperplane in the feature space and then makes different types of data lie on both sides of the hyperplane based on the confidence and empirical risk minimization principles of the data [22]. The SVM matching function is

$$f(x) = sgn\left(\sum_{i=1}^{n}\lambda_i y_i K(x_i, x) + b\right), \quad (i = 1, 2, \ldots, n) \tag{7}$$

where n represents the amount of training sample, λ represents the Lagrange multiplier, y_i is the classification label of x_i, b is the classification threshold, and $K(x_i, x)$ is the Radial Basis kernel function.

In the training and testing process for the SVM model, the normalized feature set is used as the input and the classification labels corresponding to the feature set are used as the output.

TABLE II
FEATURE CONTRIBUTION RANKING RESULTS

Air pressure	Feature contribution ranking (weakening in sequence)
1 atm	$CC_{\varphi-n}$, $Am_{\varphi-q}$, $Ku^{-}_{\varphi-q}$, $Nu_{\varphi-n}$, $Ku^{+}_{\varphi-q}$, $Sk^{-}_{\varphi-n}$, $Ku^{-}_{\varphi-n}$, $CC_{\varphi-q}$, $Ku^{+}_{\varphi-n}$, $Sk^{+}_{\varphi-q}$, $Sk^{-}_{\varphi-q}$, $Sk^{+}_{\varphi-n}$
0.5 atm	$Nu_{\varphi-n}$, $Am_{\varphi-q}$, $Ku^{+}_{\varphi-q}$, $CC_{\varphi-q}$, $Ku^{-}_{\varphi-n}$, $Ku^{+}_{\varphi-n}$, $Ku^{-}_{\varphi-q}$, $CC_{\varphi-n}$, $Sk^{+}_{\varphi-q}$, $Sk^{+}_{\varphi-n}$, $Sk^{-}_{\varphi-q}$, $Sk^{-}_{\varphi-n}$
0.1 atm	$Am_{\varphi-q}$, $Ku^{+}_{\varphi-q}$, $Nu_{\varphi-n}$, $CC_{\varphi-n}$, $Ku^{-}_{\varphi-q}$, $Ku^{-}_{\varphi-n}$, $CC_{\varphi-q}$, $Ku^{+}_{\varphi-n}$, $Sk^{-}_{\varphi-n}$, $Sk^{-}_{\varphi-q}$, $Sk^{+}_{\varphi-q}$, $Sk^{+}_{\varphi-n}$

D. Experimental Verification

According to the above-mentioned principles, the PD severity assessment of the PCB mainly includes the following steps:

1) Collecting the PRPD profile of the PCB.
2) Feature extraction of the PRPD map to form the feature vector to be evaluated.
3) Input the feature vectors to be evaluated into the trained SVM model for identification.
4) The output recognition result of the SVM model is the PD severity level, i.e., S1, S2, or S3.

In order to verify the accuracy of PD severity assessment based on fluorescent fiber detection and the importance of different PD characteristics, this article conducts validation experiments based on the built experimental platform and algorithms. Considering that the PD of PCBs may occur near different conductor structures, experiments are conducted to collect PD aging data of three PCB structures at three air pressures, respectively, for a total of 9 PCB samples with complete PD aging data. The complete PD aging data of each sample was divided into three severity stages according to the standard in Table I. Because the aging to breakdown time of each PCB sample is different, 160 PD data samples (each sample includes 1000 PD pulses) are selected uniformly from each set of complete PD aging data, of which 130 samples are used as the training set and 30 samples are used as the testing set for SVM model. Through the previous analysis for PD aging characteristics, there are differences in the aging evolution of PD characteristics at different air pressures. Therefore, the data under different air pressures are evaluated separately when conducting the severity assessment, and the PD data with different PCB structures under the same severity stage are combined together for evaluation, which can increase the rationality and generalizability of the severity assessment. Finally, there are 390 PD data samples in the training set and 90 PD data samples in the testing set for each air pressure. Each PD data sample includes 12 extracted evaluation features.

To investigate the contribution of different features on the severity assessment, the feature contribution ranking is performed with the mRMR algorithm for training datasets with 12 feature dimensions at three air pressures, and the results are shown in Table II. According to Table II, it can be seen that there is some degree of difference in the feature contribution ranking at different air pressures, which indicates that different features contribute differently to the severity assessment at different air pressures. Comparing the rankings under the three air pressures, the $Nu_{\varphi-n}$, $Am_{\varphi-q}$, $Ku^{+}_{\varphi-q}$ features are in the

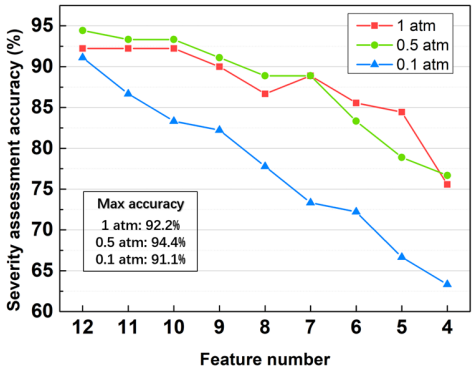

Fig. 10. Variation of PD severity assessment accuracy with the number of features at three air pressures.

top 50% of the rankings under all three air pressures, while the $Sk^{-}_{\varphi-q}$, $Sk^{+}_{\varphi-q}$, $Sk^{+}_{\varphi-n}$ features are in the bottom 50% of the rankings under all three air pressures. This phenomenon indicates that the $Nu_{\varphi-n}$, $Am_{\varphi-q}$, $Ku^{+}_{\varphi-q}$ features have high contribution under all air pressures and they can be used as the main features under multiple air pressure conditions, while the opposite is true for the $Nu_{\varphi-n}$, $Am_{\varphi-q}$, $Ku^{+}_{\varphi-q}$ features. This phenomenon also reinforces the fact that some of the PCB-related discharge characteristics currently applicable at terrestrial atmospheric pressures need to be particularly investigated in aircraft at low air pressure.

To address the effect of different numbers of features on the evaluation accuracy, we apply different numbers of features to SVM for severity assessment. Therefore, we chose the number of features from 4 to 12 for the assessment, where the reduced features are reduced one by one starting from the lowest contribution in Table II toward the features with high contribution. The results of the variation of the evaluation accuracy with the number of features at different air pressures are thus obtained, as shown in Fig. 10.

The combined use of feature extraction and SVM allows the application of some amounts of variation that cannot be directly observed visually to the severity assessment. The maximum accuracy of the severity assessment method proposed in this article can reach more than 91.1% at all three air pressures through Fig. 10, and the highest can be 94.4%, which is completely adequate for the severity assessment of PCBs. In addition, as the features with low contribution gradually decrease, the assessment accuracy also gradually decreases, which is not enough information about the category representation due to the reduction of feature information. The accuracy of the assessment at 1 and 0.5 atm air pressure decreases relatively slowly, while the accuracy of the assessment at 0.1 atm air pressure decreases more rapidly, which indicates that the number of features has a greater impact at 0.1 atm. In the case of 1 and 0.5 atm, the evaluation accuracy is still high when 10 features are used.

In addition, in a few cases, multiple PD sources may exist on the PCB at the same time, in which case the judgment of PD severity needs to consider the severity of multiple PD sources at the same time and take the most severe PD source as the basis for maintenance. Since it is difficult to achieve the simultaneous control of multiple PD sources on the PCB in the experiment, no experimental verification is done in this article. However, theoretically, the situation of multiple PD sources can be simulated by the fusion of different PRPD patterns, and then after model training, the evaluation model proposed in this article can be applied to the situation where multiple PD sources exist at the same time.

When the severity stage of the PCB is assessed as Attention Risk, at that time it might be selected to continuously observe whether the discharge is a continuous PD, so as to make further judgments. When the severity state of the PCB is Moderate Risk, the PCB surface can be selected for cleaning or other methods to improve the insulation of the PCB. When the severity state reaches Dangerous Risk, the PCB should be immediately overhauled or replaced to prevent serious accidents from occurring in advance. These assessments can also be used for factory quality control and design guidance for PCBs. Therefore, the proposed evaluation method can accurately assess the three severities of PD on PCBs at different air pressures, and also obtain the influence of different combinations of features on the evaluation, which is important for PCB health assessment and fault determination.

VI. Conclusion

In this article, a novel fluorescent fiber-based method is proposed to evaluate the severity of PD on PCBs in aircraft. Based on this method, the performance of this novel optical method at different air pressures, the PD phenomena, and characteristics of PCBs at different severity levels and the effectiveness of PD severity assessment are investigated in this article. Specifically, three main conclusions are obtained as follows:

1) A novel fluorescent fiber-based method for PD severity assessment on PCBs in aircraft is proposed. This method can effectively immunize the electromagnetic interference, acoustic interference, and vibration interference existing in the aircraft operation environment. Moreover, it can achieve an assessment accuracy of at least 91.1% and up to 94.4% under three air pressures (1, 0.5, and 0.1 atm) by using SVM algorithm. This method can accurately and reliably identify the severity of PD, and it also provides an important solution for the evaluation of PCB insulation status and the quality verification of the PCB design in aircraft.
2) Based on the optical detection method proposed in this article, the changes in surface appearance and related PD properties of PCBs during aging at three air pressures are investigated. It is found that as the PD aging intensifies, impurity deposition occurs around the copper tracks of the PCB, which accelerates the aging of the insulation to a certain extent. In addition, the optical PRPD patterns at the same air pressure show changes in distribution shape during aging, and the phase distribution range of PRPD patterns widens as the air pressure decreases. For the single optical PD pulses at different air pressures, the pulse amplitude shows a general tendency to decrease significantly and then increase slowly with aging, and the pulse interval time is found to decrease

gradually and reach a stabile value with aging. These phenomena accompanying the aging of PD provide important theoretical references for PCB PD detection and quality control, and also support our further study of the discharge mechanism.

3) In this article, 12 feature parameters are extracted for assessing the severity of PD on PCBs, which characterizes the PD aging process in terms of the PRPD pattern shape, number of pulses, discharge amplitude, and correlation. In order to investigate the contribution of different features to the assessment, the mRMR algorithm is used in this article to obtain the contribution ranking of the 12 features to the severity assessment. As a result, influence on different combinations of the feature numbers on the assessment accuracy is obtained, which facilitates the characterization of the aging process and the judgment of the feature quality in the assessment process.

REFERENCES

[1] V. Raveendran, M. Andresen, and M. Liserre, "Improving onboard converter reliability for more electric aircraft with lifetime-based control," *IEEE Trans. Ind. Electron.*, vol. 66, no. 7, pp. 5787–5796, Jul. 2019.

[2] G. Buticchi, S. Bozhko, M. Liserre, P. Wheeler, and K. Al-Haddad, "On-board microgrids for the more electric aircraft—Technology review," *IEEE Trans. Ind. Electron.*, vol. 66, no. 7, pp. 5588–5599, Jul. 2019.

[3] M. Borghei and M. Ghassemi, "Insulation materials and systems for more- and all-electric aircraft: A review identifying challenges and future research needs," *IEEE Trans. Transport. Electrific.*, vol. 7, no. 3, pp. 1930–1953, Sep. 2021.

[4] B. Du, Y. Liu, and H. Liu, "Effects of low pressure on tracking failure of printed circuit boards," *IEEE Trans. Dielectr. Electr. Insul.*, vol. 15, no. 5, pp. 1379–1384, Oct. 2008.

[5] W. Cao, B. C. Mecrow, G. J. Atkinson, J. W. Bennett, and D. J. Atkinson, "Overview of electric motor technologies used for more electric aircraft (MEA)," *IEEE Trans. Ind. Electron.*, vol. 59, no. 9, pp. 3523–3531, Sep. 2012.

[6] S. S. Yeoh, M. Rashed, M. Sanders, and S. Bozhko, "Variable-voltage bus concept for aircraft electrical power system," *IEEE Trans. Ind. Electron.*, vol. 66, no. 7, pp. 5634–5643, Jul. 2019.

[7] M. Borghei and M. Ghassemi, "Classification of partial discharge in electric aircraft based on short-term behavior of insulation systems," in *Proc. AIAA*, 2021, p. 3294.

[8] S.-W. Jee, "The effect of guard on improving the resistance to tracking phenomenon for the PCB," *J. Electr. Eng. Technol.*, vol. 17, no. 1, pp. 485–494, Jan. 2022.

[9] A. Cavallini, L. Versari, and L. Fornasari, "Feasibility of partial discharge detection in inverter-fed actuators used in aircrafts," in *Proc. Annu. Rep. Conf. Electr. Insul. Dielectric Phenomena*, Oct. 2013, pp. 1250–1253.

[10] J. Jiang et al., "Optical sensing of partial discharge in more electric aircraft," *IEEE Sensors J.*, vol. 20, no. 21, pp. 12723–12731, Nov. 2020.

[11] Z. Wei et al., "Study of partial discharge behavior at flight-altitude pressures under 60 Hz and impulse voltages for samples related to aircraft motors," in *Proc. IEEE Int. Power Modulator High Voltage Conf. (IPMHVC)*, Jun. 2018, pp. 180–185.

[12] C. Emersic, R. Lowndes, I. Cotton, S. Rowland, and R. Freer, "Degradation of conformal coatings on printed circuit boards due to partial discharge," *IEEE Trans. Dielectr. Electr. Insul.*, vol. 23, no. 4, pp. 2232–2240, Aug. 2016.

[13] C. Emersic, R. Lowndes, I. Cotton, S. Rowland, and R. Freer, "The effects of pressure and temperature on partial discharge degradation of silicone conformai coatings," *IEEE Trans. Dielectr. Electr. Insul.*, vol. 24, no. 5, pp. 2986–2994, Oct. 2017.

[14] G. G. Karady, M. D. Sirkis, and J. R. Oliva, "Degrading effect of high-altitude corona on electronic circuit boards," *IEEE Trans. Electr. Insul.*, vol. 26, no. 6, pp. 1216–1219, 1991.

[15] E. Zeynali, R. Bridges, and B. Kordi, "Investigation of partial discharge in aircraft conformally-coated printed circuit boards," in *Proc. IEEE Electr. Insul. Conf. (EIC)*, Jun. 2019, pp. 30–33.

[16] Y. Zang et al., "Optical detection method for partial discharge of printed circuit boards in electrified aircraft under various pressures and voltages," *IEEE Trans. Transport. Electrific.*, vol. 8, no. 4, pp. 4668–4677, Dec. 2022.

[17] D. McCarthy et al., "Radiation dosimeter using an extrinsic fiber optic sensor," *IEEE Sensors J.*, vol. 14, no. 3, pp. 673–685, Mar. 2014.

[18] J. Jiang, M. Zhao, Z. Wen, C. Zhang, and R. Albarracín, "Detection of DC series arc in more electric aircraft power system based on optical spectrometry," *High Voltage*, vol. 5, no. 1, pp. 24–29, Feb. 2020.

[19] E. Zeynali, R. Bridges, and B. Kordi, "Electrical insulation of conformally coated printed circuit boards: An overview and a study of the influence of pollution," *IEEE Elect. Insul. Mag.*, vol. 37, no. 2, pp. 6–17, Mar. 2021.

[20] H. Schefer, L. Fauth, T. H. Kopp, R. Mallwitz, J. Friebe, and M. Kurrat, "Discussion on electric power supply systems for all electric aircraft," *IEEE Access*, vol. 8, pp. 84188–84216, 2020.

[21] H. Peng, F. Long, and C. Ding, "Feature selection based on mutual information criteria of max-dependency, max-relevance, and min-redundancy," *IEEE Trans. Pattern Anal. Mach. Intell.*, vol. 27, no. 8, pp. 1226–1238, Aug. 2005.

[22] A. Mathur and G. M. Foody, "Multiclass and binary SVM classification: Implications for training and classification users," *IEEE Geosci. Remote Sens. Lett.*, vol. 5, no. 2, pp. 241–245, Apr. 2008.

Yiming Zang was born in Shandong, China, in 1996. He received the B.E. degree in electrical engineering from Southwest Jiao Tong University, Chengdu, China, in 2018, and the Ph.D. degree in electrical engineering from Shanghai Jiao Tong University, Shanghai, China, in 2022.

He is currently an Assistant Research Fellow with the School of Electrical Engineering, Shanghai Jiao Tong University. His research interests include online monitoring and fault diagnosis for power equipment insulation.

Mohamad Ghaffarian Niasar was born in Tehran, Iran, in 1984. He received the M.Sc. degree from the Sharif University of Technology, Tehran, in 2008, and the Ph.D. degree in electrical engineering from the Royal Institute of Technology (KTH), Stockholm, Sweden, in 2015.

He is currently an Assistant Professor with DC System, Energy Conversion and Storage group with the Delft University of Technology, Delft, The Netherlands. His main research interests are aging of electrical insulation, HVdc insulation system, partial discharges, high frequency power transformers, power cables, and FEM modeling.

Ze Li was born in Shandong, China, in 1997. She received the B.E. degree in electrical engineering from North China Electric Power University, Baoding, China, in 2019. She is currently pursuing the Ph.D. degree in electrical engineering with Shanghai Jiao Tong University, Shanghai, China.

Her research interests include optical detection and fault diagnosis of partial discharge.

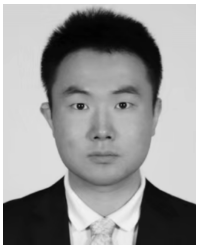

Yaocheng Li received the bachelor's degree in electrical engineering from Southwest Jiaotong University, Chengdu, China, in 2018. He is currently pursuing the Ph.D. degree with Shanghai Jiao Tong University, Shanghai, China.

His current research interest includes computer vision-based autonomous defect detection in power transmission equipment.

Qinglin Qian received the master's degree from Shandong University, Jinan, China. He is currently pursuing the Ph.D. degree with Shanghai Jiao Tong University, Shanghai, China.

His research interests include online monitoring of power equipment.

Xiuchen Jiang was born in Shandong, China, in 1965. He received the B.E. degree in electrical engineering from Shanghai Jiao Tong University, Shanghai, China, in 1987, the M.S. degree in high voltage and insulation technology from Tsinghua University, Beijing, China, in 1992, and the Ph.D. degree in electrical engineering from Shanghai Jiao Tong University in 2001.

He is currently a Professor with the Department of Electrical Engineering, Shanghai Jiao Tong University. His research interests include online monitoring, condition-based maintenance, and automation for electrical equipment.

Peter Vaessen (Member, IEEE) was born in Maasbree, The Netherlands, in 1960. He received the M.Sc. degree (cum laude) in electrical power engineering from Eindhoven Technical University, Eindhoven, The Netherlands, in 1985.

In 1985, he joined KEMA (now a CESI brand), The Netherlands. In his 35-year career, he held research positions in the field of large power transformers and high voltage measurement and testing. He is an Innovations Manager at KEMA Laboratories and the Chairperson of the European Distributed Energy Resources Laboratories Association (DERlab), as well as a member of several national and international working groups. Since 2017 he is Part-Time Professor Hybrid Transmission Systems at the Delft University of Technology (TU Delft), Delft, The Netherlands, where he teaches high voltage technology and HVdc.